Journal of Applied Analysis and Computation
Volume 16, Number 4, August 2026, 1860–1883
Website:http://www.jaac-online.com
DOI:10.11948/20250348

INSTABILITY-DRIVEN PATTERN FORMATION IN A NETWORK SIR MODEL WITH INDIRECT TRANSMISSION AND QUASI-LAPLACIAN DIFFUSION*

Wenjie Gu[1,2], Qianqian Zheng[2,†] and Jianwei Shen[1,†]

Abstract This study investigates how indirect transmission and diffusion asymmetry shape epidemic dynamics in a network-organized SIR model. Using linear stability analysis and eigenmode decomposition, we derive explicit conditions for Hopf bifurcation, Turing instability, and their interaction. The results show that indirect transmission significantly shifts epidemic thresholds, while asymmetric diffusion across network nodes promotes the activation of additional eigenmodes and the emergence of spatially heterogeneous infection patterns. Numerical simulations on random and quasi-Laplacian networks reveal transitions among stable equilibria, periodic outbreaks, and mixed Hopf-Turing regimes, with the specific pattern determined jointly by biological parameters and network topology. To validate the theory, the model was calibrated using real influenza surveillance data from 44 countries. The observed periodicity and spatial clustering closely match the model predictions, demonstrating that instability-driven mechanisms can explain real-world influenza oscillations and heterogeneity. These findings provide a unified theoretical and data-supported framework for understanding epidemic pattern formation and designing interventions that target indirect transmission and mobility-induced spatial instabilities.

Keywords SIR epidemic model, pattern formation, Hopf bifurcation, turing instability, indirect transmission.

MSC(2010) 34D10, 34D20, 34N05.

1. Introduction

Real-world populations interact within structured social or spatial networks, where epidemic transmission is shaped not only by direct contacts but also by indirect pathways, such as imported cases, environmental contamination, and anomalous diffusion. These factors lead to dynamics that significantly deviate from classical well-mixed compartmental models [1]. Early COVID-19 forecasting studies further highlighted that even under strong interventions, epidemic trajectories may exhibit identifiable turning points and plateau phases that require mechanism-informed fitting and prediction beyond simple well-mixed assumptions [9]. To address these complexities, a variety of mathematical frameworks have been developed. For instance, fractional-

†The corresponding authors.
[1]School of Mathematics and Statistics, North China University of Water Resources and Electric Power, Jinshui East Road, Zhengzhou 450046, China
[2]School of Science, Xuchang University, 88 Bayi Road, Xuchang 461000, China
*The authors were supported by National Natural Science Foundation of China (12272135, 11971416) and National Science Foundation of Henan (242300420661).
Email: X20241080774@stu.ncwu.edu.cn(W. Gu), zqq@xcu.edu.cn(Q. Zheng), phdshen@126.com(J. Shen)

order models incorporating nonlinear incidence and quarantine effects reveal memory-dependent influences on epidemic persistence [5], while infection-age-structured SIS systems exhibit rich oscillatory behaviors through Hopf bifurcation analysis [15]. Spatial diffusion further induces Turing instabilities, generating heterogeneous epidemic hotspots [20]. Network structures and time delays introduce additional layers of complexity, with SIS and SIR models demonstrating thresholds, periodic waves, and spatiotemporal patterns, often analyzed via Lyapunov methods and delay differential equation theory [21, 24], non-autonomous delayed epidemic models have also been used to produce long-term predictions of confirmed and deceased cases in China, illustrating the practical forecasting relevance of delay-structured dynamics [10]. Moreover, Turing instabilities driven by delays and connectivity can explain recurrent epidemic oscillations and inform control strategies [22]. Recently, higher-order network topology and temporal network structures have been shown to substantially reshape epidemic propagation and control outcomes, enabling richer spatiotemporal pattern dynamics beyond pairwise static contacts [25, 27]. In addition, data-driven propagation modeling coupled with intelligent algorithms has gained attention for capturing complex spreading processes under heterogeneous environments [23], related data-driven diagnosis studies using spectral analysis of cough recordings demonstrate how signal-based learning can complement mechanistic epidemic modeling in real-world surveillance pipelines [7]. While, studies also explore the interplay between disease and information dynamics in multiplex networks, showing that preventive information raises epidemic thresholds, whereas misinformation lowers them [12]. Control-oriented approaches, such as stochastic SEIR models with distributed delays, enable outbreak suppression through Lyapunov-based sliding mode controllers and stochastic bifurcation analysis [17]. Extensions of SIR models further investigate recurrence, optimal control, and cluster synchronization on coupled networks, illustrating how viral states influence synchronization and transmission dynamics [13, 26].

Building on these foundations, reaction-diffusion and network-based studies have advanced our understanding of how mobility, cross-diffusion, degree heterogeneity, and modularity shape epidemic thresholds and persistence. These works clarify the extension of Hopf and Turing mechanisms to network Laplacians via eigenmode selection [11, 16]. For example, Turing instability in large random networks can lead to spontaneous node differentiation into activator-rich and activator-poor groups, resulting in multi-stationary states and hysteresis that differ from classical continuous-media patterns [8]. Normal form theory applied to Hopf bifurcations in network-organized reaction-diffusion systems reveals that network topology critically influences the emergence of spatially nonhomogeneous periodic patterns, as seen in predator-prey models [4]. Extensions to directed networks uncover topology-driven instabilities that generate traveling waves or quasi-stationary structures absent in undirected systems [2]. In discrete-time systems, transitions and coexistence among spiral waves, Turing patterns, and Turing-like states can occur, with strong impulse noise exciting novel patterning through competition among stable equilibria [14]. Within epidemic contexts, network-organized SIR models demonstrate that the maximum eigenvalue of the network matrix, governed by connectivity and infection rates, controls outbreak thresholds and Turing instabilities, with validations using COVID-19 data [18]. Related analyses of enzyme-catalyzed reactions and delayed epidemic systems highlight how equilibrium classification, Laplacian spectra, and memory effects drive complex spatiotemporal instabilities and chaotic outbreaks [3, 19]. Despite these advances, which demonstrate how network topology, diffusion asymmetry, and delays enrich Hopf-Turing instabilities to produce oscillations, multi-stationary states, and complex patterns beyond continuous-media models, significant gaps remain. Most existing studies examine temporal oscillations or spatial heterogeneity in isolation, often overlooking the combined role of indirect transmission pathways and

quasi-Laplacian coupling in triggering and sustaining bifurcations. This is particularly relevant given their central importance in biological and epidemiological systems, where indirect effects and asymmetric diffusion interact with network heterogeneity to shape epidemic dynamics.

In this work, we extend the classical SIR paradigm by incorporating indirect transmission effects and quasi-Laplacian coupling into a generalized network framework. Leveraging bifurcation theory and normal form reduction, we systematically analyze the emergence and interaction of Hopf and Turing instabilities under heterogeneous network structures. Our theoretical results, corroborated by numerical simulations on random networks, delineate the conditions for transitions between disease-free states, endemic equilibria, and oscillatory or spatially heterogeneous epidemic patterns. By elucidating the interplay among indirect transmission pathways, network heterogeneity, and diffusion asymmetry, this study deepens the theoretical understanding of epidemic pattern formation and offers practical insights into intervention strategies for managing outbreaks in structured populations.

2. The generalized network-organized SIR systems with the indirect effect

In this paper, we study the following network-organized SIR model with the indirect effect

$$\begin{aligned} \frac{dS_i(t)}{dt} &= f(S_i, I_i) + d_S \sum_{j=1}^{n} L_{ij}(S_j - u), \\ \frac{dI_i(t)}{dt} &= g(S_i, I_i) + d_I \sum_{j=1}^{n} L_{ij}(I_j - v), \end{aligned} \tag{2.1}$$

where the model is defined as $f(S,I) = \alpha - \beta S^2 - \gamma SI^2$, $g(S,I) = \beta S^2 + \gamma SI^2 - \delta I$ with S_i and I_i $(i = 1, 2, \ldots, n)$ denoting the densities of susceptible and infected individuals at the i-th node. The parameters characterize biological and diffusive processes: α represents susceptibility, β corresponds to indirect transmission, for example, during the COVID-19 pandemic, the virus spreads indirectly through intermediate carriers such as objects and environmental surfaces, γ reflects infection driven by external factors, δ accounts for recovery or removal, and d_1, d_2 are the diffusion rates of susceptibles and infectives, respectively. $L = A - \varepsilon diag\{k_1, k_2, ..., k_n\}$, $k_i (i = 1, 2, 3, ..., n)$ is the degree of node, ε can be treated as the disturbance intensity. A denotes the adjacency matrix of the network, where $A_{ij} = 1$ if nodes i and j are connected, and $A_{ij} = 0$ otherwise. The coupling matrix $L = A - \varepsilon diag\{k_1, k_2, ..., k_n\}$ is a real symmetric matrix (a quasi-Laplacian), and thus its eigenvalues Λ_i are all real and can be ordered as $\{\Lambda_{n_t} : \Lambda_1 > \Lambda_{n_1} > \Lambda_{n_2} > \cdots > \Lambda_{n_m}\}$. $u = \frac{-\gamma\,\alpha^2 + \sqrt{\alpha^4\gamma^2 + 4\,\alpha\,\beta\,\delta^4}}{2\,\beta\,\delta^2}, v = \frac{\alpha}{\delta}$ are the equilibrium, where $f(u,v) = g(u,v) = 0$. Although the equations primarily track the densities of susceptible S and infected I individuals, the model retains the structure of an SIR process where recovery is modeled via the term $-\delta I$. Hence, we maintain the SIR nomenclature to align with the classical epidemiological paradigm.

Linearizing system (2.1) at the equilibrium (u, v), we obtain

$$\frac{dS_i(t)}{dt} = (-\gamma\,v^2 - 2\,\beta\,u)S_i + (-2\,\gamma\,uv)I_i + d_S \sum_{j=1}^{n} L_{ij}S_j,$$

$$\frac{dI_i(t)}{dt} = (\gamma\, v^2 + 2\,\beta\, u)S_i + (2\,\gamma\, uv - \delta)I_i + d_I \sum_{j=1}^{n} L_{ij} I_j,$$

and the linearizing system can be written as

$$\frac{dC}{dt} = (E_n \otimes A(\beta))C + (L \otimes D)C,$$

where E_n is unit matrix, L is the Laplacian matrix, $A(\beta)$ is the Jacobian matrix without network, D is the coupling strength matrix, $C = (S_1, I_1, ..., S_n, I_n)^T$,

$$A(\beta) = \begin{pmatrix} -\gamma\, v^2 - 2\,\beta\, u & -2\,\gamma\, uv \\ \gamma\, v^2 + 2\,\beta\, u & 2\,\gamma\, uv - \delta \end{pmatrix}, D = \begin{pmatrix} d_S & 0 \\ 0 & d_I \end{pmatrix},$$

$$J(\beta) = E_n \otimes A(\beta) + L \otimes D,$$

$$J_i(\beta) = A(\beta) + \Lambda_i D,$$

and λ_i, Λ_i are the eigenvalue of $J_i(\beta), L$, respectively; $C_i = (C_{i1}, C_{i2})^T, \phi^{(1)} = (\phi_1^{(1)}, \phi_2^{(1)}, ..., \phi_n^{(1)})$ are the corresponding eigenvector, satisfying

$$J_i(\beta)C_i = \lambda_i C_i,$$
$$L\phi^{(1)} = \Lambda_i \phi^{(1)}.$$

Then, we know λ_i and $\phi^{(i)} \otimes C_i$ are the eigenvalue and eigenvector of $J(\beta)$, respectively, because

$$\begin{aligned} J(\beta)(\phi^{(1)} \otimes C_i) &= (E_n \otimes A(\beta) + L \otimes D)(\phi^{(1)} \otimes C_i) \\ &= (E_n \otimes A(\beta))(\phi^{(1)} \otimes C_i) + (L \otimes D)(\phi^{(1)} \otimes C_i) \\ &= (E_n \phi^{(1)}) \otimes (A(\beta)C_i) + (L\phi^{(1)}) \otimes (DC_i) \\ &= \phi^{(1)} \otimes (A(\beta)C_i) + (\Lambda_i \phi^{(1)}) \otimes (DC_i) \\ &= \phi^{(1)} \otimes (A(\beta)C_i) + \phi^{(1)} \otimes ((\Lambda_i D)C_i) \\ &= \phi^{(1)} \otimes (A(\beta)C_i + (\Lambda_i D)C_i) \\ &= \phi^{(1)} \otimes ((A(\beta) + \Lambda_i D)C_i) \\ &= \phi^{(1)} \otimes (J_i(\beta)C_i) \\ &= \phi^{(1)} \otimes (\lambda_i C_i) \\ &= \lambda_i(\phi^{(1)} \otimes C_i). \end{aligned}$$

Therefore, we just consider the stability of system (2.1) through ith node, and the corresponding characteristic equation can be written as

$$\lambda^2 - E_i(\beta)\lambda + F_i(\beta) = 0, \tag{2.2}$$

where

$$E_i(\beta) = -\gamma v^2 - 2\beta u + 2\gamma uv - \delta + \Lambda_i(d_S + d_I),$$
$$F_i(\beta) = \Lambda^2 d_I d_S + \left(-d_I \gamma v^2 + 2 d_S \gamma uv - 2\beta d_I u - \delta d_S\right)\Lambda + \delta\gamma v^2 + 2\beta\delta u,$$

and the eigenvalues $\lambda(\beta)$ are given by

$$\lambda(\beta) = \frac{E_i(\beta) \pm \sqrt{E_i^2(\beta) - 4F_i(\beta)}}{2}.$$

Based on the Hopf bifurcation criterion, system (2.1) undergoes a Hopf bifurcation at $\beta = \beta_c$ provided that

$$E_i(\beta_c) = 0, F_i(\beta_c) > 0, E_i'(\beta_c) \neq 0, \tag{2.3}$$

and $E_j(\beta_c) \neq 0, F_j(\beta_c) \neq 0$ for $i \neq j$, which make only one Hopf bifurcation occur.

The unique pair of complex eigenvalues can be expressed as $a(\beta) \pm ib(\beta)$, $a(\beta) = \frac{E_i(\beta)}{2}$, $b(\beta) = \frac{\sqrt{4F_i(\beta) - E_i(\beta)^2}}{2}$. In the following, we consider the sign of $a'(\beta_c) = \frac{E_i'(\beta)}{2}|_{\beta=\beta_c}$, and obtain

$$E_i'(\beta) = -\frac{\alpha(G_1 - G_2)}{2\beta^2\delta^3\sqrt{\alpha\ (\gamma^2\alpha^3 + 4\beta\delta^4)}}, \tag{2.4}$$

where $G_1 = \gamma^3\alpha^4 + 2\gamma\alpha\delta^4\beta + 2\delta^5\beta^2, G_2 = \gamma^2\sqrt{\alpha\ (\gamma^2\alpha^3 + 4\beta\delta^4)}\alpha^2$. We know the sign of $E_i'(\beta)$ is determined by $G_1 - G_2$, and $G_1^2 - G_2^2 = 4\gamma^3\alpha^4\beta^2\delta^5 + 4\gamma^2\alpha^2\beta^2\delta^8 + 8\gamma\alpha\beta^3\delta^9 + 4\beta^4\delta^{10} > 0$. And these roots of $E_i'(\beta) = 0$ are $\beta_1 = \frac{\gamma\alpha}{\delta^3}\left(\sqrt{-\delta\gamma}\alpha - \delta^2\right)$, $\beta_2 = -\frac{\gamma\alpha}{\delta^3}\left(\sqrt{-\delta\gamma}\alpha + \delta^2\right)$, and β_1, β_2 are complex roots, namely, no real roots of $E_i'(\beta) = 0$ exist. Therefore, $E_i'(\beta) < 0 (a'(\beta_c) < 0)$ always holds, namely, $a(\beta)$ is monotonic decreasing with β.

Based on these above analysis, we have

Theorem 2.1. (Hopf bifurcation) *For system (2.1) without network, Hopf bifurcation occurs at β_c; system is stable when $\beta > \beta_c$ and unstable(periodic) when $\beta < \beta_c$.*

Proof. The process can be found in the above analysis. □

Finally, we consider the Turing instability by $F_i(\beta) < 0$ when $\beta > \beta_c$. $F_i(\beta)$ is a quadratic equation with an opening upwards. Let $\sigma = \frac{d_S}{d_I} > 0$, at $\Lambda_c = -\frac{-v^2\gamma - 2\beta u + (2\gamma uv - \delta)\sigma}{2 d_S}$, we obtain

$$F_{\min} = F_{\min}(\beta, \Lambda_c)\sigma = r_1\sigma^2 + r_2\sigma + r_3, \tag{2.5}$$

where $r_1 = -\gamma^2u^2v^2 + \delta\gamma uv - \frac{\delta^2}{4}, r_2 = \gamma^2uv^3 + 2\beta\gamma u^2v + \frac{\delta\gamma v^2}{2} + \beta\delta u, r_3 = -\frac{\gamma^2v^4}{4} - \beta\gamma uv^2 - \beta^2u^2$.

Suppose $\sigma_1 = \frac{-r_2 - \sqrt{r_2^2 - 4r_1r_3}}{2r_1}$ and $\sigma_2 = \frac{-r_2 + \sqrt{r_2^2 - 4r_1r_3}}{2r_1}$ are the roots of $F_{\min}(\beta, \sigma) = 0$. If $r_1 > 0$, $F_{\min}(\beta, \Lambda_c)\sigma < 0$ when $\sigma \in (\sigma_1, \sigma_2)$; If $r_1 < 0$, $F_{\min}(\beta, \Lambda_c)\sigma < 0$ when $\sigma \in (-\infty, \sigma_1) \cup (\sigma_2, +\infty)$.

Theorem 2.2. (Turing bifurcation) *For system (2.1), Turing bifurcation occurs at σ_c ($F_{\min}(\beta, \sigma_c) = 0$); Turing instability region of σ is (σ_1, σ_2) when $r_1 > 0$ and $(-\infty, \sigma_1) \cup (\sigma_2, +\infty)$ when $r_1 < 0$.*

Proof. The process can be found in the above analysis. □

Assume $\tau_1, \tau_2 (\tau_1 < \tau_2)$ are the roots of $F_i(\beta) = 0$ on basis of Theorem 2.2.

Theorem 2.3. (Turing instability) *For system (2.1), Turing instability occurs when* $(\tau_1, \tau_2) \cap \Lambda_{n_t} \neq \emptyset$.

Proof. When $\Lambda_i \in (\tau_1, \tau_2)$, $F_i(\beta, \Lambda_i) = {\Lambda_i}^2 d_I\, d_S + (-d_I\, \gamma\, v^2 + 2\, d_S\, \gamma\, uv - 2\, \beta\, d_I\, u - \delta\, d_S)\Lambda_i + \delta\, \gamma\, v^2 + 2\, \beta\, \delta\, u < 0$ holds and at least one eigenvalue with positive real part exists in system (2.2), namely, Turing instability occurs in system (2.1). □

3. Normal form analysis in network-organized system

To investigate the stability and bifurcation direction, we consider system (2.1) at the critical value $\beta = \beta_c$, which takes the form

$$\frac{dC}{dt} = J(\beta_c)C + N(C), \tag{3.1}$$

where

$$C = \begin{pmatrix} C_1 \\ \vdots \\ C_n \end{pmatrix}, C_i = \begin{pmatrix} S_i \\ I_i \end{pmatrix},$$

$$N(C) = E_n \otimes \begin{pmatrix} f_{SS}(u,v)S^2 + f_{SI}(u,v)SI + f_{II}(u,v)I^2 + f_{SII}(u,v)SI^2 \\ g_{SS}(u,v)S^2 + g_{SI}(u,v)SI + g_{II}(u,v)I^2 + g_{SII}(u,v)SI^2 \end{pmatrix}$$

and $f_{SS}(u,v) = -2\beta, f_{SI}(u,v) = -2\gamma v, f_{II}(u,v) = -2\gamma u, f_{SII}(u,v) = -2\gamma$, $g_{SS}(u,v) = 2\beta, g_{SI}(u,v) = 2\gamma v, g_{II}(u,v) = 2\gamma u, g_{SII}(u,v) = 2\gamma$, and $f_{SSI} = f_{SSS} = f_{III} = g_{SSI} = g_{SSS} = g_{III} = 0$.

By calculating

$$J(\beta_c)\begin{pmatrix} p_1 \\ q_1 \end{pmatrix} = ib(\beta_c)\begin{pmatrix} p_1 \\ q_1 \end{pmatrix}, (J(\beta_c))^T\begin{pmatrix} p_2 \\ q_2 \end{pmatrix} = -ib(\beta_c)\begin{pmatrix} p_2 \\ q_2 \end{pmatrix}$$

and $\langle p^*, p\rangle = 1$, we obtain

$$p = \phi^{(1)} \otimes \begin{pmatrix} p_1 \\ q_1 \end{pmatrix} = \phi^{(1)} \otimes \begin{pmatrix} 1 \\ \dfrac{-\gamma\, v^2 + d_S\, \Lambda - 2\, \beta\, u - ib\beta_c}{2\, \gamma\, uv} \end{pmatrix},$$

$$p^* = \phi^{(1)} \otimes \begin{pmatrix} p_2 \\ q_2 \end{pmatrix} = \phi^{(1)} \otimes \begin{pmatrix} \dfrac{p_{21}\Lambda^2 + p_{22}\Lambda + p_{23}}{p_{24}\Lambda^2 + p_{25}\Lambda + p_{26}}, \\ \dfrac{q_{21}\Lambda + q_{22}}{q_{23}\Lambda^2 + q_{24}\Lambda + q_{25}} \end{pmatrix},$$

where $\langle p^*, \overline{p}\rangle = 0$, $\phi^{(1)}$ is the eigenvector of the eigenvalue Λ_1 who induces the Hopf bifurcation, also, the specific values of the detailed expressions are presented in the appendix A1.

Theorem 3.1. *System (3.1) is equivalent to*

$$\begin{aligned}\frac{dz}{dt} &= ib(\beta_c)z + \langle p^*, N_c\rangle,\\ \frac{d\omega}{dt} &= J(\beta_c)\omega + H(z,\overline{z},\omega).\end{aligned}$$

Proof. We decompose $R^{2n} = T^c \oplus T^{su}$ with $T^c = \{zp+\overline{zp}|z\in\mathbb{C}\}$ and $T^{su} = \{C\in R^{2n}|\langle p^*, C\rangle = 0\}$. For any $C = (S_1, I_1, ..., S_n, I_n)^T$, there is $z\in\mathbb{C}$ and $\omega = (\omega_1^{(S)}, \omega_1^{(I)}, ..., \omega_n^{(S)}, \omega_n^{(I)})^T$ such that $z = \langle p^*, C\rangle$,

$$C = zp + \overline{zp} + \omega, \tag{3.2}$$

by differentiating both sides of the equation (3.2), we obtain

$$\begin{aligned}\frac{dC}{dt} &= \frac{dz}{dt}p + \frac{d\overline{z}}{dt}\overline{p} + \frac{d\omega}{dt},\\ \frac{dC}{dt} &= J(\beta_c)C + N(C),\end{aligned} \tag{3.3}$$

applying the inner product to both sides of equation (3.3) with respect to p^*, we have

$$\begin{aligned}\langle p^*, \frac{dC}{dt}\rangle &= \frac{dz}{dt}\langle p^*, p\rangle + \frac{d\overline{z}}{dt}\langle p^*, \overline{p}\rangle + \langle p^*, \frac{d\omega}{dt}\rangle = \frac{dz}{dt},\\ \langle p^*, \frac{dC}{dt}\rangle &= \langle p^*, J(\beta_c)C + N(C)\rangle\\ &= \langle p^*, J(\beta_c)(zp + \overline{zp} + \omega)\rangle + \langle p^*, N_c(C)\rangle\\ &= \langle p^*, J(\beta_c)zp\rangle + \langle p^*, J(\beta_c)\overline{zp}\rangle + \langle p^*, J(\beta_c)\omega\rangle + \langle p^*, N_c(C)\rangle\\ &= ib(\beta_c)z\langle p^*, p\rangle - ib(\beta_c)\overline{z}\langle p^*, \overline{p}\rangle + \langle p^*, N_c(C)\rangle\\ &= ib(\beta_c)z + \langle p^*, N_c\rangle,\end{aligned}$$

namely,

$$\frac{dz}{dt} = ib(\beta_c)z + \langle p^*, N_c\rangle.$$

Substituting system (3.2) into (3.3), we obtain

$$\begin{aligned}&\frac{d(zp + \overline{zp} + \omega)}{dt} = J(\beta_c)(zp + \overline{zp} + \omega) + N(zp + \overline{zp} + \omega)\\ \Rightarrow &\frac{dz}{dt}p + \frac{d\overline{z}}{dt}\overline{p} + \frac{d\omega}{dt} = zJ(\beta_c)p + \overline{z}J(\beta_c)\overline{p} + J(\beta_c)\omega + N(zp + \overline{zp} + \omega)\\ \Rightarrow &ib(\beta_c)zp + p\langle p^*, N_c\rangle - ib(\beta_c)\overline{zp} + \overline{p}\langle\overline{p^*}, N_c\rangle + \frac{d\omega}{dt} = zib(\beta_c)p + \overline{z}(-ib(\beta_c))\overline{p}\\ &\qquad + J(\beta_c)\omega + N(zp + \overline{zp} + \omega)\\ \Rightarrow &\frac{d\omega}{dt} = J(\beta_c)\omega + N(zp + \overline{zp} + \omega) - \langle p^*, N_c\rangle p - \langle\overline{p^*}, N_c\rangle\overline{p},\end{aligned}$$

and we have

$$\frac{d\omega}{dt} = J(\beta_c)\omega + H(z,\overline{z},\omega),$$

where $H(z,\overline{z},\omega)=N_c-\langle p^*,N_c\rangle p-\langle\overline{p^*},N_c\rangle\overline{p}$ and $N_c=N_c(zp+\overline{zp}+\omega)$.

According to the above analysis, system (3.1) is equivalent to

$$\begin{aligned}\frac{dz}{dt}&=ib(\beta_c)z+\langle p^*,N_c\rangle,\\ \frac{d\omega}{dt}&=J(\beta_c)\omega+H(z,\overline{z},\omega).\end{aligned}\tag{3.4}$$

□

In the following, we consider the high order term $\langle p^*,N_c\rangle, H(z,\overline{z},\omega)$. And the general form of N_c can be expressed as

$$N_c=\frac{1}{2}K(C,C)+\frac{1}{6}M(C,C,C)+O(|C|^4),$$

where $K(X,Y)$ and $M(X,Y,Z)$ are multilinear functions, $K_{XY}=K_i(X,Y)=\sum\limits_{j,k=1}^{n}\frac{\partial^2N_i(\xi)}{\partial\xi_j\partial\xi_k}|_{\xi=0}x_jy_k$, and $M_{XYZ}=M_i(X,Y,Z)=\sum\limits_{j,k,l=1}^{n}\frac{\partial^3N_i(\xi)}{\partial\xi_j\partial\xi_k\partial\xi_l}|_{\xi=0}x_jy_kz_l$, $i=1,2,...,n$.

To consider $K(X,Y)$ and $M(X,Y,Z)$, we rewrite system (3.2) as

$$\begin{aligned}S_i&=zp_n\phi_i^{(1)}+\overline{zp_n}\phi_i^{(1)}+\omega_i^{(S)},\\ I_i&=zq_n\phi_i^{(1)}+\overline{zq_n}\phi_i^{(1)}+\omega_i^{(I)},\end{aligned}$$

and $K(zp+\overline{zp},zp+\overline{zp})=z^2K(p,p)+2z\overline{z}K(p,\overline{p})+\overline{z}^2K(\overline{p},\overline{p})$,

$$\begin{aligned}K(p,p)&=(\cdots,(\phi_i^{(1)})^2c_1,(\phi_i^{(1)})^2d_1,\cdots)^T,\\ K(p,\overline{p})&=(\cdots,(\phi_i^{(1)})^2e_1,(\phi_i^{(1)})^2f_1,\cdots)^T,\\ M(p,p,\overline{p})&=(\cdots,(\phi_i^{(1)})^3g_1,(\phi_i^{(1)})^3h_1,\cdots)^T,\end{aligned}$$

where

$$\begin{aligned}c_1&=f_{SS}p_1^2+2f_{SI}p_1q_1+f_{II}q_1^2=a_{11}\Lambda^2+a_{12}\Lambda+a_{13},\\ d_1&=g_{SS}p_1^2+2g_{SI}p_1q_1+g_{II}q_1^2=a_{21}\Lambda^2+a_{22}\Lambda+a_{23},\\ e_1&=f_{SS}p_1\overline{p_1}+f_{SI}(p_1\overline{q_1}+\overline{p_1}q_1)+f_{II}(q_1\overline{q_1})=a_{31}\Lambda^2+a_{32}\Lambda+a_{33},\\ f_1&=g_{SS}p_1\overline{p_1}+g_{SI}(p_1\overline{q_1}+\overline{p_1}q_1)+g_{II}(q_1\overline{q_1})=a_{41}\Lambda^2+a_{42}\Lambda+a_{43},\\ g_1&=f_{SSS}p_1\overline{p_1}p_1+f_{SSI}(2p_1\overline{p_1}q_1+p_1^2\overline{q_1})+f_{SII}(2q_1\overline{q_1}p_1+q_1^2\overline{p_1})+f_{III}q_1\overline{q_1}q_1\\ &=a_{51}\Lambda^2+a_{52}\Lambda+a_{53},\\ h_1&=g_{SSS}p_1\overline{p_1}p_1+g_{SSI}(2p_1\overline{p_1}q_1+p_1^2\overline{q_1})+g_{SII}(2q_1\overline{q_1}p_1+q_1^2\overline{p_1})+g_{III}q_1\overline{q_1}q_1\\ &=a_{61}\Lambda^2+a_{62}\Lambda+a_{63},\end{aligned}$$

and the detailed values of the expressions are presented in the appendix A2.

In order to obtain the expression of $H(z,\overline{z},\omega)$, we expand $H(z,\overline{z},\omega)$ as

$$H(z,\overline{z},\omega)=\frac{H_{20}}{2}z^2+H_{11}z\overline{z}+\frac{H_{02}}{2}\overline{z}^2+o(|z|^3)+o(|z|\cdot|\omega|),$$

and according to the definition of $H(z,\overline{z},\omega)$, one has

$$\begin{aligned}H(z,\overline{z},\omega) &= N_c - \langle p^*, N_c\rangle p - \langle \overline{p^*}, N_c\rangle \overline{p}\\ &= \frac{1}{2}z^2(K_{pp} - \langle p^*, K_{pp}\rangle p - \langle \overline{p^*}, K_{pp}\rangle \overline{p})\\ &\quad + z\overline{z}(K_{p\overline{p}} - \langle p^*, k_{p\overline{p}}\rangle p - \langle \overline{p^*}, K_{p\overline{p}}\rangle \overline{p}) + \frac{1}{2}\overline{z}^2(K_{\overline{pp}} - \langle p^*, K_{\overline{pp}}\rangle p - \langle \overline{p^*}, K_{\overline{pp}}\rangle \overline{p}) + \cdots.\end{aligned}$$

Comparing these coefficients of $H(z,\overline{z},\omega)$, we obatin

$$\begin{aligned}H_{20} &= K_{pp} - \langle P^*, K_{pp}\rangle p - \langle \overline{p^*}, K_{pp}\rangle \overline{p},\\ H_{11} &= K_{p\overline{p}} - \langle P^*, K_{p\overline{p}}\rangle p - \langle \overline{p^*}, K_{p\overline{p}}\rangle \overline{p},\end{aligned}$$

where

$$\begin{aligned}\langle p^*, K_{pp}\rangle &= (\overline{p_2}c_1 + \overline{q_2}d_1)s_3 = \frac{b_{12}b_{13}}{b_{11}}s_3,\\ \langle \overline{p^*}, K_{pp}\rangle &= (p_2c_1 + q_2d_1)s_3 = \frac{b_{22}b_{23}}{b_{21}}s_3,\\ \langle p^*, K_{p\overline{p}}\rangle &= (\overline{p_2}e_1 + \overline{q_2}f_1)s_3 = \frac{b_{32}b_{33}}{b_{31}}s_3,\\ \langle \overline{p^*}, K_{p\overline{p}}\rangle &= (p_2e_1 + q_2f_1)s_3 = \frac{b_{42}b_{43}}{b_{41}}s_3,\\ \langle p^*, M_{pp\overline{p}}\rangle &= (\overline{p_2}g_1 + \overline{q_2}h_1)s_4 = \frac{b_{52}b_{53}b_{54}}{b_{51}}s_4,\end{aligned}$$

and the values of the specific expressions can be found in the appendix A3.

Theorem 3.2. *Assume the form of ω is*

$$\omega = \frac{\omega_{20}}{2}z^2 + \omega_{11}z\overline{z} + \frac{\omega_{02}}{2}\overline{z}^2 + o(|z|^3), \langle p^*, \omega_{i,j}\rangle = 0,\ i,j = 0,1,2, i+j = 2 \tag{3.5}$$

we can obtain

$$\begin{aligned}\omega_{20} &= [E_n \otimes (2ib(\beta_c)E_2) - J(\beta_c)]^{-1}H_{20},\\ \omega_{11} &= -[J(\beta_c)]^{-1}H_{11},\end{aligned}$$

and

$$\begin{aligned}\langle p^*, K(p,w_{11})\rangle &= -\langle p^*, K(p, J(\beta_c)^{-1}K(p,\overline{p}))\rangle + \langle p^*, K(p,p)\rangle\frac{\langle p^*, K(p,\overline{p})\rangle}{ib(\beta_c)}\\ &\quad - \frac{|\langle \overline{p^*}, K(p,\overline{p})\rangle|^2}{ib(\beta_c)},\\ \langle p^*, K(\overline{p},w_{20})\rangle &= \langle p^*, K(\overline{p}, (2ib(\beta_c)E_2 - J(\beta_c))^{-1}K(p,p))\rangle\\ &\quad - \langle p^*, K(\overline{p},p)\rangle\frac{\langle p^*, K(p,p)\rangle}{ib(\beta_c)} - \frac{|\langle p^*, K(\overline{p},\overline{p})\rangle|^2}{3ib(\beta_c)}.\end{aligned}$$

Proof. Differentiating both sides of the equation (3.5), we obtain

$$\begin{aligned}\frac{d\omega}{dt} &= 2z\frac{dz}{dt}\frac{\omega_{20}}{2} + \omega_{11}(\overline{z}\frac{dz}{dt} + z\frac{d\overline{z}}{dt}) + 2\frac{\omega_{02}}{2}\overline{z}\frac{dz}{dt} + o(|z|^3)\\ &= ib(\beta_c)z^2\omega_{20} + ib(\beta_c)z\overline{z}(\omega_{11} - \omega_{11}) - ib(\beta_c)\overline{z}^2\omega_{02} + o(|z|^3)\\ &= ib(\beta_c)z^2\omega_{20} - ib(\beta_c)\overline{z}^2\omega_{02} + o(|z|^3)\end{aligned} \tag{3.6}$$

also, we know

$$\begin{aligned}\frac{d\omega}{dt} &= J(\beta_c)\omega + H(z,\overline{z},\omega)\\ &= J(\beta_c)(\frac{\omega_{20}}{2}z^2 + \omega_{11}z\overline{z} + \frac{\omega_{02}}{2}\overline{z}^2) + \frac{H_{20}}{2}z^2 + H_{11}z\overline{z} + \frac{H_{02}}{2}\overline{z}^2\\ &= (\frac{J(\beta_c)\omega_{20}}{2} + \frac{\omega_{20}}{2})z^2 + (J(\beta_c)\omega_{11} + H_{11})z\overline{z} + (\frac{J(\beta_c)\omega_{02}}{2} + \frac{H_{02}}{2})\overline{z}^2.\end{aligned} \tag{3.7}$$

Comparing the coefficients between system (3.6) and (3.7), we have

$$\begin{aligned}&ib(\beta_c)\omega_{20} = \frac{J(\beta_c)}{2}\omega_{20} + \frac{H_{20}}{2} \Rightarrow \omega_{20} = [E_n \otimes (2ib(\beta_c)E_2) - J(\beta_c)]^{-1}H_{20},\\ &J(\beta_c)\omega_{11} + H_{11} = 0 \Rightarrow \omega_{11} = -[J(\beta_c)]^{-1}H_{11}.\end{aligned}$$

Namely,

$$\begin{aligned}\omega_{20} &= [E_n \otimes (2ib(\beta_c)E_2) - J(\beta_c)]^{-1}H_{20},\\ \omega_{11} &= -[J(\beta_c)]^{-1}H_{11}.\end{aligned} \tag{3.8}$$

On basis of the relationship between the eigenvalue and the eigenvector

$$\begin{aligned}&J(\beta_c)^{-1}p = \frac{1}{ib(\beta_c)}p,\ \ J(\beta_c)^{-1}\overline{p} = -\frac{1}{ib(\beta_c)}\overline{p},\\ &(2ib(\beta_c)E_2 - J(\beta_c))^{-1}p = \frac{1}{ib(\beta_c)}p,\ \ (2ib(\beta_c)E_2 - J(\beta_c))^{-1}\overline{p} = \frac{1}{3ib(\beta_c)}\overline{p},\end{aligned}$$

we have

$$\begin{aligned}J(\beta_c)^{-1}H_{11} &= J(\beta_c)^{-1}(K(p,\overline{p}) - \langle p^*, K(p,\overline{p})\rangle p - \langle \overline{p^*}, K(p,\overline{p})\rangle \overline{p})\\ &= J(\beta_c)^{-1}K(p,\overline{p}) - \langle p^*, K(p,\overline{p})\rangle \frac{p}{ib(\beta_c)} + \langle \overline{p^*}, K(p,\overline{p})\rangle \frac{\overline{p}}{ib(\beta_c)},\end{aligned}$$

and

$$\begin{aligned}&(2ib(\beta_c)E_2 - J(\beta_c))^{-1}H_{20}\\ =&(2ib(\beta_c)E_2 - J(\beta_c))^{-1}(K(p,p) - \langle p^*, K(p,p)\rangle p - \langle \overline{p^*}, K(p,p)\rangle \overline{p})\\ =&(2ib(\beta_c)E_2 - J(\beta_c))^{-1}K(p,p) - \langle p^*, K(p,p)\rangle \frac{p}{ib(\beta_c)} - \langle \overline{p^*}, K(p,p)\rangle \frac{\overline{p}}{3ib(\beta_c)}.\end{aligned}$$

Furthermore, we obtain

$$\begin{aligned}&\langle p^*, K(p, w_{11})\rangle\\ =& -\langle p^*, K(p, J(\beta_c)^{-1}H_{11})\rangle\\ =& k - \langle p^*, K(p, J(\beta_c)^{-1}K(p,\overline{p}) - \langle p^*, K(p,\overline{p})\rangle \frac{p}{ib(\beta_c)} + \langle \overline{p^*}, K(p,\overline{p})\rangle \frac{\overline{p}}{ib(\beta_c)})\rangle\\ =& -\langle p^*, K(p, J(\beta_c)^{-1}K(p,\overline{p}))\rangle + \langle p^*, K(p,p)\rangle \frac{\langle p^*, K(p,\overline{p})\rangle}{ib(\beta_c)} - \frac{|\langle \overline{p^*}, K(p,\overline{p})\rangle|^2}{ib(\beta_c)},\end{aligned}$$

and

$$\begin{aligned}
&\langle p^*, K(\overline{p}, w_{20})\rangle \\
&= \langle p^*, K\left(\overline{p}, (2ib(\beta_c)E_2 - J(\beta_c))^{-1}H_{20}\right)\rangle \\
&= \langle p^*, K\left(\overline{p}, (2ib(\beta_c)E_2 - J(\beta_c))^{-1}K(p,p) - \langle p^*, K(p,p)\rangle\frac{p}{ib(\beta_c)} - \langle \overline{p^*}, K(p,p)\rangle\frac{\overline{p}}{3ib(\beta_c)}\right)\rangle \\
&= \langle p^*, K\left(\overline{p}, (2ib(\beta_c)E_2 - J(\beta_c))^{-1}K(p,p)\right)\rangle - \langle p^*, K(\overline{p},p)\rangle\frac{\langle p^*, K(p,p)\rangle}{ib(\beta_c)} - \frac{|\langle p^*, K(\overline{p},\overline{p})\rangle|^2}{3ib(\beta_c)}.
\end{aligned}$$

□

Substituting system (3.5) into system (3.4), we have

$$\begin{aligned}
\frac{dz}{dt} =& ib(\beta_c)z + \frac{1}{2}g_{20}z^2 + g_{11}z\overline{z} + \frac{1}{2}g_{02}\overline{z}^2 + \frac{1}{6}g_{30}z^3 \\
&+ \frac{1}{2}g_{21}z^2\overline{z} + \frac{1}{2}g_{12}z\overline{z}^2 + \frac{1}{6}g_{03}\overline{z}^3 + O(|z|^4)
\end{aligned} \tag{3.9}$$

where the specific derivation process of the formula in A4,

$$\begin{aligned}
g_{20} &= \langle p^*, K(p,p)\rangle, \\
g_{11} &= \langle p^*, K(p,\overline{p})\rangle, \\
g_{02} &= \langle p^*, K(\overline{p},\overline{p})\rangle, \\
g_{30} &= 3\langle p^*, K(p,\omega_{20})\rangle + \langle p^*, M(p,p,p)\rangle), \\
g_{21} &= 2\langle p^*, K(p,\omega_{11})\rangle + \langle p^*, K(\overline{p},\omega_{20})\rangle + \langle p^*, M(p,p,\overline{p})\rangle, \\
g_{12} &= 2\langle p^*, K(\overline{p},\omega_{11})\rangle + \langle p^*, K(p,\omega_{02})\rangle + \langle p^*, M(p,\overline{p},\overline{p})\rangle, \\
g_{03} &= 3\langle p^*, K(\overline{p},\omega_{02})\rangle + \langle p^*, M(\overline{p},\overline{p},\overline{p})\rangle.
\end{aligned}$$

Theorem 3.3. *For the form of z, system (3.9) can be transformed into*

$$\frac{d\omega}{dt} = ib(\beta_c)\omega + c_1\omega^2\overline{\omega} + O(|\omega|^4).$$

Proof. The process will be given through Lemma 3.1 and Lemma 3.2.

Lemma 3.1. *For $\beta = \beta_c$,*

$$\frac{dz}{dt} = ib(\beta_c)z + \frac{g_{20}}{2}z^2 + g_{11}z\overline{z} + \frac{g_{02}}{2}\overline{z}^2 + O(|z|^3)$$

can be transferred to

$$\frac{d\omega}{dt} = ib(\beta_c)\omega + O(|\omega|^3)$$

by

$$z = \omega + \frac{h_{20}}{2}\omega^2 + h_{11}\omega\overline{\omega} + \frac{h_{02}}{2}\overline{\omega}^2. \tag{3.10}$$

□

Proof. The inverse transformation can be expressed as

$$\omega = z - \frac{h_{20}}{2}z^2 - h_{11}z\overline{z} - \frac{h_{02}}{2}\overline{z}^2 + O(|z|^3),$$

then

$$\begin{aligned}\frac{d\omega}{dt} &= \frac{dz}{dt} - h_{20}z\frac{dz}{dt} - h_{11}\left(\frac{dz}{dt}\overline{z} + z\frac{d\overline{z}}{dt}\right) - h_{02}\overline{z}\frac{d\overline{z}}{dt} + \cdots \\ &= ib(\beta_c)z + \left(\frac{g_{20}}{2} - ib(\beta_c)h_{20}\right)z^2 + \left(g_{11} - ib(\beta_c)h_{11} - \overline{ib(\beta_c)}h_{11}\right)z\overline{z} \\ &\quad + \left(\frac{g_{02}}{2} - \overline{ib(\beta_c)}h_{02}\right)\overline{z}^2 + \cdots \\ &= ib(\beta_c)\omega + \frac{1}{2}\left(g_{20} - ib(\beta_c)h_{20}\right)\omega^2 + \left(g_{11} - \overline{ib(\beta_c)}h_{11}\right)\omega\overline{\omega} \\ &\quad + \frac{1}{2}\left(g_{02} - 2\overline{ib(\beta_c)} + ib(\beta_c)h_{02}\right)\overline{\omega}^2 + O(|\omega|^3).\end{aligned}$$

Let

$$h_{20} = \frac{g_{20}}{ib(\beta_c)}, h_{11} = \frac{g_{11}}{-ib(\beta_c)}, h_{02} = \frac{g_{02}}{-3ib(\beta_c)},$$

we have

$$\frac{d\omega}{dt} = ib(\beta_c)\omega + O(|\omega|^3).$$

□

Lemma 3.2. *For $\beta = \beta_c$,*

$$\frac{dz}{dt} = ib(\beta_c)z + \frac{g_{30}}{6}z^3 + \frac{g_{21}}{2}z^2\overline{z} + \frac{g_{12}}{2}z\overline{z}^2 + \frac{g_{03}}{6}\overline{z}^3 + O(|z|^4)$$

can be transferred to

$$\frac{d\omega}{dt} = ib(\beta_c)\omega + c_1(\beta_c)\omega^2\overline{\omega} + O(|\omega|^4)$$

through

$$z = \omega + \frac{h_{30}}{6}\omega^3 + \frac{h_{21}}{2}\omega^2\overline{\omega} + \frac{h_{12}}{2}\omega\overline{\omega}^2 + \frac{h_{03}}{6}\overline{\omega}^3.$$

Proof. The inverse transformation can be expressed as

$$\omega = z - \frac{h_{30}}{6}z^3 - \frac{h_{21}}{2}z^2\overline{z} - \frac{h_{12}}{2}z\overline{z}^2 - \frac{h_{03}}{6}\overline{z}^3 + O(|z|^4),$$

then

$$\begin{aligned}\frac{d\omega}{dt} &= \frac{dz}{dt} - \frac{h_{30}}{2}z^2\frac{dz}{dt} - \frac{h_{21}}{2}\left(2z\overline{z}\frac{dz}{dt} + z^2\frac{d\overline{z}}{dt}\right) - \frac{h_{12}}{2}\left(\frac{dz}{dt}\overline{z}^2 + 2z\overline{z}\frac{d\overline{z}}{dt}\right) - \frac{h_{03}}{2}\overline{z}^2\frac{d\overline{z}}{dt} + \cdots \\ &= ib(\beta_c)z + \left(\frac{g_{30}}{6} - \frac{ib(\beta_c)h_{30}}{2}\right)z^3 + \left(\frac{g_{21}}{2} - ib(\beta_c)h_{21} - \frac{\overline{ib(\beta_c)}h_{21}}{2}\right)z^2\overline{z} \\ &\quad + \left(\frac{g_{12}}{2} - \frac{ib(\beta_c)h_{21}}{2} - \overline{ib(\beta_c)}h_{12}\right)z\overline{z}^2 + \left(\frac{g_{03}}{6} - \frac{\overline{ib(\beta_c)}h_{03}}{2}\right)\overline{z}^3 + \cdots \\ &= ib(\beta_c)\omega + \frac{1}{6}\left(g_{30} - 2ib(\beta_c)h_{30}\right)\omega^3 + \frac{1}{2}\left(g_{21} - (ib(\beta_c) + \overline{ib(\beta_c)})h_{21}\right)\omega^2\overline{\omega} \\ &\quad + \frac{1}{2}\left(g_{12} - 2\overline{ib(\beta_c)}h_{12}\right)\omega\overline{\omega}^2 + \frac{1}{6}\left(g_{03} + (ib(\beta_c) - 3\overline{ib(\beta_c)})h_{03}\right)\overline{\omega}^3 + O(|\omega|^4).\end{aligned}$$

Let

$$h_{30} = \frac{g_{30}}{2ib(\beta_c)}, h_{12} = \frac{g_{12}}{-2ib(\beta_c)}, h_{03} = \frac{g_{03}}{-4ib(\beta_c)},$$

we have

$$\frac{d\omega}{dt} = ib(\beta_c)\omega + c_1(\beta_c)\omega^2\overline{\omega} + O(|\omega|^4).$$

□

In the following, we try to determine the expression of $c_1(\beta_c)$. Substituting system (3.10) into system (3.9), we have

$$\begin{aligned}\frac{dz}{dt} &= ib(\beta_c)\omega + \frac{g_{20}}{2}\left(2h_{11}\omega^2\overline{\omega}\right) + g_{11}\left(\overline{h_{11}}\omega^2\overline{\omega} + \frac{h_{20}}{2}\omega^2\overline{\omega}\right) + \frac{g_{02}}{2}h_{02}\omega^2\overline{\omega} + \frac{g_{21}}{2}\omega^2\overline{\omega} \\ &= ib(\beta_c)\omega + \left(\frac{(2ib(\beta_c) + \overline{ib(\beta_c)})g_{20}g_{11}}{2|ib(\beta_c)|^2} + \frac{|g_{11}|^2}{ib(\beta_c)} + \frac{|g_{02}|^2}{2(2ib(\beta_c) - \overline{ib(\beta_c)})} + \frac{g_{21}}{2}\right)\omega^2\overline{\omega},\end{aligned}$$

then

$$\begin{aligned}c_1(\beta_c) &= \frac{(2ib(\beta_c) + \overline{ib(\beta_c)})g_{20}g_{11}}{2|ib(\beta_c)|^2} + \frac{|g_{11}|^2}{ib(\beta_c)} + \frac{|g_{02}|^2}{2(2ib(\beta_c) - \overline{ib(\beta_c)})} + \frac{g_{21}}{2} \\ &= \frac{i}{b(\beta_c)}\left(\frac{g_{20}g_{11}}{2} - |g_{11}|^2 - \frac{|g_{02}|^2}{6}\right) + \frac{g_{21}}{2},\end{aligned} \tag{3.11}$$

where $g_{20}, g_{11}, \frac{g_{21}}{2}, g_{02}$ can be found in Theorem 3.1 and Theorem 3.2.

In a similar way, the normal form for $\beta \to \beta_c$ can be written as

$$\frac{d\omega}{dt} = \lambda(\beta)\omega + c_1(\beta)\omega^2\overline{\omega} + O(|\omega|^4),$$

where

$$c_1(\beta) = \frac{(2\lambda + \overline{\lambda})g_{20}g_{11}}{2|\lambda|^2} + \frac{|g_{11}|^2}{\lambda} + \frac{|g_{02}|^2}{2(2\lambda - \overline{\lambda})} + \frac{g_{21}}{2}.$$

□

According to Ref. [6, 8], we have the following theorem.

Theorem 3.4. *For the network-organized system (2.1), the Hopf bifurcation is subcritical when* $Re(c_1(\beta)) > 0$ *and supercritical when* $Re(c_1(\beta)) < 0$. *The bifurcation yields stable periodic orbits if* $Re(c_1(\beta)) < 0$, *while it is unstable when* $Re(c_1(\beta)) > 0$. *Moreover, the periodic solutions are spatially homogeneous provided that* $|\phi_i^{(1)}| < 0.1$ [8] *for all* $i = 1, 2, \ldots, n$ *together with* $Re(c_1(\beta)) < 0$; *in contrast, they become spatially nonhomogeneous if some* $|\phi_i^{(1)}| > 0.1$ *and* $Re(c_1(\beta)) > 0$ *hold.*

4. Numerical results and discussion

In this section, numerical simulations are carried out to validate the theoretical results and illustrate the biological mechanisms. The computations use a time step $h = 0.01$ with the fourth-order Runge–Kutta method, and the parameters are set as $\alpha = 0.35$, $\beta = 0.05$, $\gamma = 1.1$, and $\delta = 1$. The network topology used is an Erdös-Rényi (ER) random graph with a fixed number of nodes $n = 100$. The parameter p denotes the probability of connection between any two distinct nodes, with $p \in [0, 1]$. Each figure and result presented is based on a single

representative random network realization, chosen because the qualitative dynamical behavior including bifurcation thresholds and pattern types was consistently observed across different random instances with the same parameters.

According to Theorem 2.1, system (2.1) without network is periodic [Figure 1(a)] when $\beta = 0.01 < \beta_c = 0.0449$ is less, which means the outbreak of infectious diseases is periodic state. When $\beta_c < \beta = 0.05$, it's stable [Figure 1(b)], which means the endemic state. Namely, the indirect effect has become one of the dominating factors of the outbreak behaviors [Figure 1(c)]. With the variation of parameters, different outbreak states of the epidemic can be observed. When the birth rate of the susceptible is low or zero, system (2.1) remains stable, corresponding to the epidemic or disease-free state. However, as the birth rate gradually increases, system (2.1) transitions from a stable state to a periodic state at $\alpha_c = 0.372$, which corresponds to a shift from an endemic state to periodic outbreaks of the disease [Figure 2(a)]. The direct infection rate similarly affects the dynamical behaviors of the spread; system (2.1) exhibits a periodic state [Figure 2(b)] when the direct infection rate reaches certain levels, representing periodic outbreaks. The recovery rate also plays a critical role in transitions from an endemic state to periodic outbreaks, the system exhibits periodic oscillations when $\delta < \delta_c = 1.7$ and stable when $\delta > \delta_c = 1.7$ [Figure 2(c)]. Meanwhile, the number of infected individuals decreases with its gradual increase, eventually leading to a disease-free state. In biological mechanism, when transmission is weak, the interplay between susceptible replenishment and infection depletion produces predator-prey-like oscillations, leading to periodic outbreaks; stronger transmission stabilizes the endemic equilibrium as indirect effects dominate. Similarly, an increased birth rate of the susceptible or a higher direct infection rate can drive a Hopf bifurcation, shifting the system from a stable endemic state to oscillatory outbreaks, while a higher recovery rate enhances damping, suppresses oscillations, and eventually eliminates infection. These mechanisms explain how parameter variations govern transitions among periodic, endemic, and disease-free states, consistent with the epidemiological dynamics.

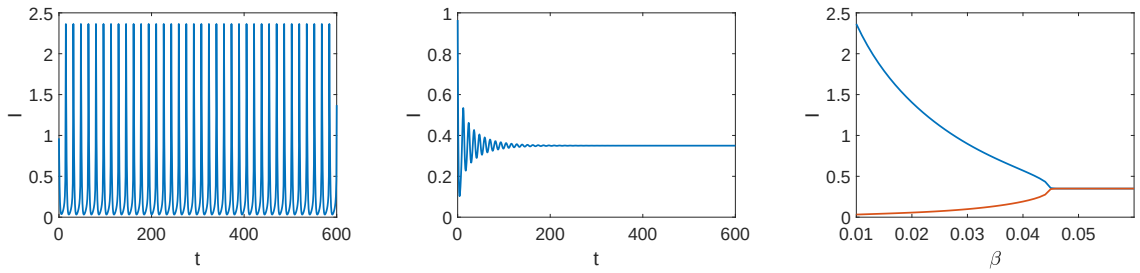

Figure 1. The stability of system (2.1) without network. (a) Hopf bifurcation occurs and system is periodic when $\beta = 0.01$. (b) The system is stable when $\beta = 0.05$. (c) The bifurcation about β.

According to Theorem 2.2 and Theorem 2.3, we consider Turing bifurcation and Turing instability when $F_{\min} \leq 0$. It was calculated that $\sigma_1 = 0.066, \sigma_2 = 21.53$ and $\Lambda_c = -\frac{-0.2969+0.2487\sigma}{2\sigma}$. In this paper, we mainly investigate the effect of network on Turing instability by the Laplacian matrix. Therefore, Λ_c should be non-positive and Turing instability occurs when $\sigma > \sigma_2$ [Figure 3(a)]. When $d_S = 3, d_I = 0.1, \sigma = 30 > \sigma_2$ and Turing instability may occur [Figure 3(b)]. When $d_S = 2, d_I = 0.1, \sigma = 20 < \sigma_2$ and Turing instability never occur [Figure 3(c)]. Next, we show the condition of Turing instability for some special network. Figure 4(a) shows $(\tau_1, \tau_2) \cap \Lambda_{n_t} \neq \emptyset$

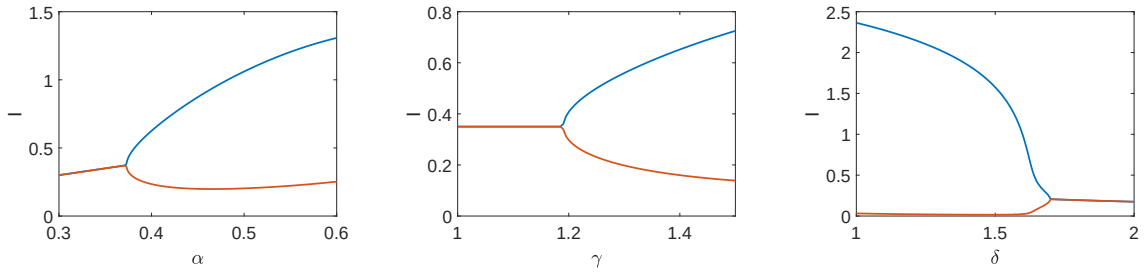

Figure 2. The bifurcation of system (2.1) without network. (a) The bifurcation about α. (b) The bifurcation about γ. (c) The bifurcation about δ.

and the pattern shows coexistence of periodic, endemic, and disease-free states [Figure 4(b)]. When $(\tau_1, \tau_2) \cap \Lambda_{n_t} = \emptyset$ [Figure 4(c)], the pattern is homogeneous [Figure 4(d)]. In Figure 4, it's found that instability mode (the eigenvalues Λ make $F_i(\beta) < 0$) could induce Turing instability and reorganize the distribution of infectious diseases again. According to Theorem 2.1 and Theorem 2.3, only Hopf bifurcation occurs [Figure 5(a)] when $\beta = 0.02, d_S = 2, d_I = 0.1, p = 0.2$, the corresponding pattern is periodic [Figure 5(b)]. Both Hopf bifurcation and Turing bifurcation occur when $\beta = 0.02, d_S = 2, d_I = 0.1, p = 0.02$, the corresponding pattern is periodic in time and is not synchronous in space. Namely, Turing-Hopf bifurcation could induce more complex phenomena.

The number of instability mode varies with p [Figure 6(a)] and more instability modes will be obtained when $\varepsilon < 1$ [Figure 6(b)]. It is found that $\beta_c(\Lambda)$ is proportional to Λ [Figure 6(c)] at Hopf bifurcation point, which mean $\varepsilon < 1$ could extend the periodic region of infectious disease and make the periodic outbreak easier. Epidemiologically, Turing instability arises when the susceptible moves much faster than the infective, continuously feeding local outbreaks while infections remain localized, thereby generating spatially heterogeneous epidemic hot-spots instead of homogeneous prevalence. The underlying network structure plays a decisive role: If Laplacian eigenvalues lie within the instability interval, specific structural modes are amplified, producing non-uniform epidemic distributions, while the absence of such eigenvalues preserves homogeneity. As network parameters such as connectivity or heterogeneity increase, the number of instability modes grows, giving rise to more diverse and complex spatial epidemic patterns, including coexistence of periodic outbreaks, endemic states, and disease-free regions. From a control perspective, limiting rapid susceptible movement, isolating or transferring the infective, and restructuring contact networks (e.g., reducing cross-community links or balancing connectivity) can effectively suppress instability modes and mitigate spatial epidemic clustering.

On the basis of Theorem 2.1 and Theorem 3.4, we further examined the periodic behaviors of infectious diseases with respect to the indirect infection rate β. For $\varepsilon = 1$, the pattern formation is stable periodic [Figure 7(a)] when $\beta = 0.0449$ and $Re(c_1(\beta)) = -0.0070 < 0$; although the amplitude become larger when $\beta = 0.035$; the pattern formation is stable [Figure 7(b)] because $Re(c_1(\beta)) = -0.0038 < 0$ holds. Meanwhile, the critical eigenvector associated with $\Lambda_1 = 0$ at $\beta_c = 0.0449$ is spatially uniform [Figure 7(c)], leading to homogeneous periodic solutions [Figure 7(a,b)], which is consistent with the numerical results [8]. In contrast, Figure 8 shows that the eigenvector corresponding to the dominant eigenvalue $\Lambda_1 = 2.0304$ becomes spatially heterogeneous, giving rise to nonuniform periodic outbreaks when $\beta = 0.035$ [Figure 8(a)] or $\beta = 0.01$ [Figure 8(b)]. Namely, for $\varepsilon < 1$, the pattern formation becomes nonuniform periodic

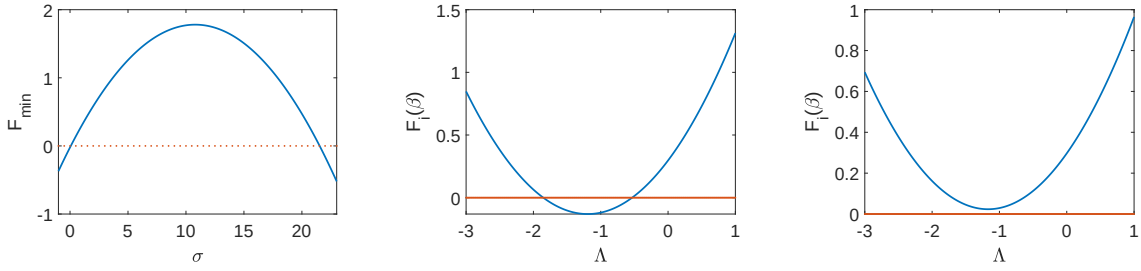

(a) (b) (c)

Figure 3. The instability condition of system (2.1). (a) The minimum with $\sigma = \frac{d_S}{d_I}$. (b) The distribution of $F_i(\beta)$ with Λ when $d_S = 3, d_I = 0.1$. (c) The distribution of $F_i(\beta)$ with Λ when $d_S = 2, d_I = 0.1$.

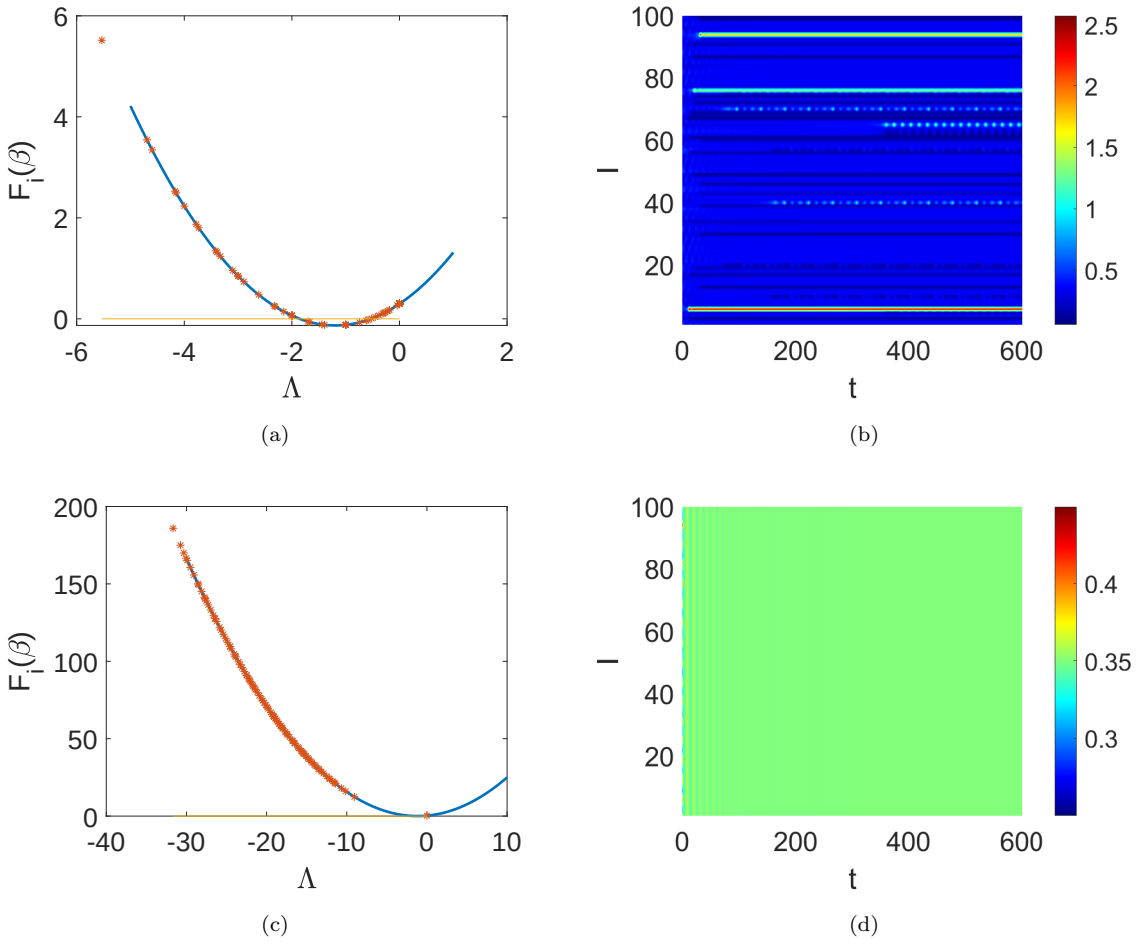

(a) (b) (c) (d)

Figure 4. Turing instability and pattern formation of system (2.1) when $d_I = 0.1$. (a) The distribution of Λ when $d_S = 3, p = 0.01$. (b) The pattern formation when $d_S = 3, p = 0.01$. (c) The distribution of Λ when $d_S = 2, p = 0.2$. (d) The pattern formation when $d_S = 2, p = 0.2$.

when $\beta = 0.035$ and $Re(c_1(\beta)) = 0.0017 > 0$, and the periodic amplitude will be larger when $\beta = 0.01$ and $Re(c_1(\beta)) = 0.0137 > 0$. Also, the stability of pattern formation is in line with

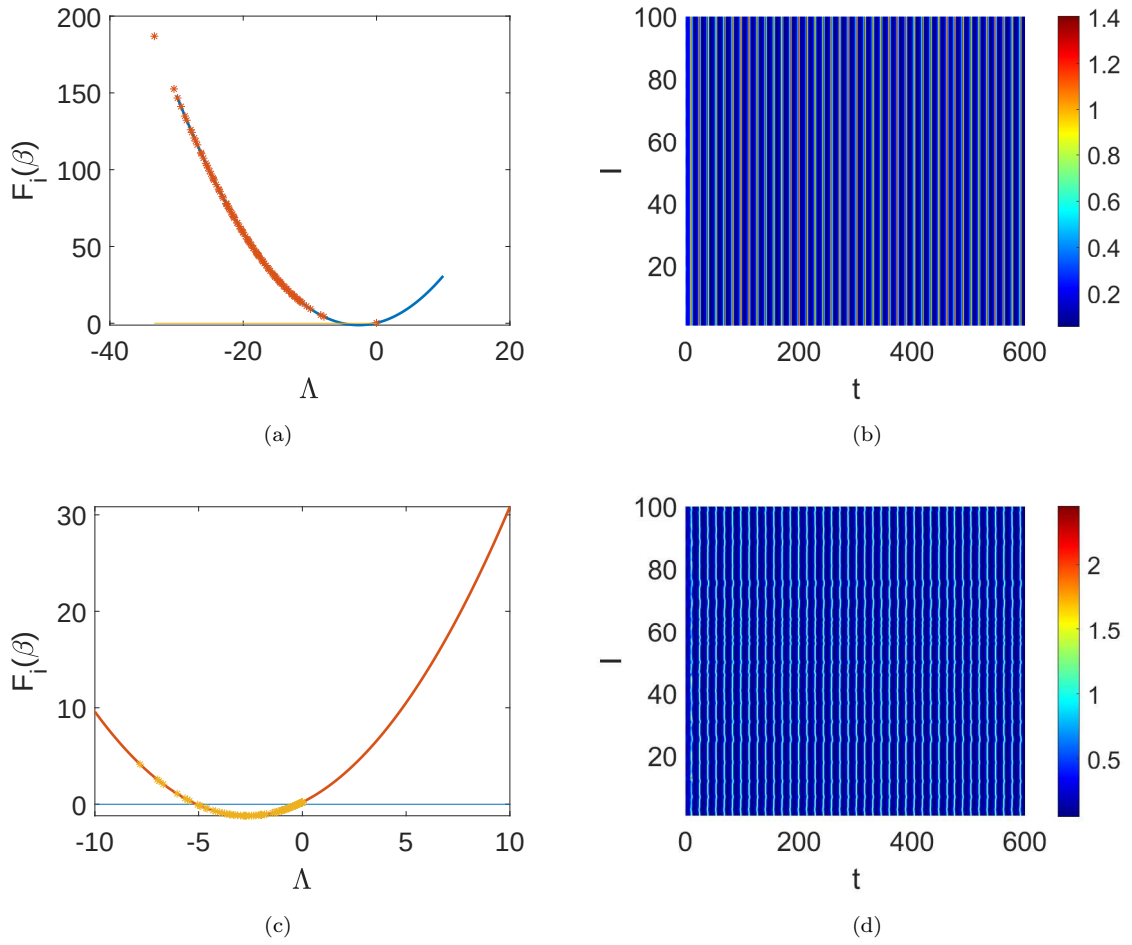

Figure 5. The instability and pattern formation of system (2.1) when $\beta = 0.02, d_S = 2, d_I = 0.1$. (a) The distribution of Λ when $p = 0.2$. (b) The pattern formation when $p = 0.2$. (c) The distribution of Λ when $p = 0.02$. (d) The pattern formation when $p = 0.02$.

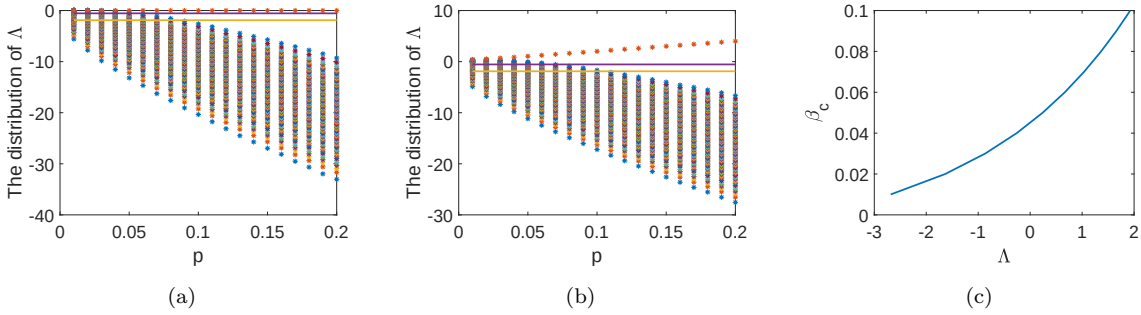

Figure 6. The distribution of Λ. (a) The distribution of Λ for Laplacian matrix $\varepsilon = 1$. (b) The distribution of Λ for Quasi-Laplacian matrix $\varepsilon = 0.8$. (c) The relationship between Λ and β_c.

the distribution of the eigenvector [8] and the stability periodic solutions. These observations are consistent with Theorem 3.4 and Ref. [8], which shows that the direction and stability of

Hopf bifurcations are determined by the cubic coefficient $c_1(\beta)$ in the normal form: A supercritical Hopf bifurcation with $\mathrm{Re}(c_1(\beta)) < 0$ produces stable, sustained oscillations, whereas a subcritical Hopf bifurcation with $\mathrm{Re}(c_1(\beta)) > 0$ leads to unstable periodic states. From an epidemiological perspective, the results imply that homogeneous network structures favor synchronous oscillations across all nodes, while heterogeneous networks amplify specific eigenmodes and generate localized epidemic hotspots. Thus, quasi-Laplacian coupling not only increases the number of instability modes but also shifts the Hopf bifurcation toward spatially nonhomogeneous outbreaks, thereby facilitating the coexistence of periodic epidemics and endemic states in structured populations. Subsequently, we utilized specific influenza data from 44 countries across three regions Africa, the Mediterranean, and the Western Pacific over nearly four years from 11.14.2021 to 10.12.2025 to verify our theoretical results. In data processing, we replaced certain missing specific values in the influenza data of these countries with 0 and performed unified standardization to ensure all values fall within a consistent range. The obtained pattern results show that influenza in most nodes (countries) exhibits periodic [Figure 9], which corresponds to our theoretical findings.

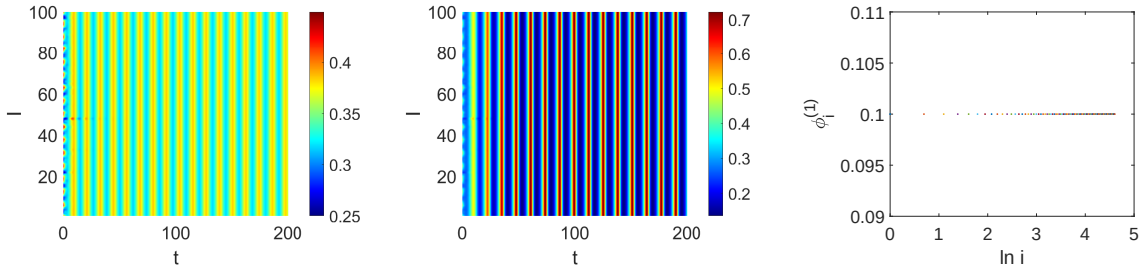

Figure 7. The pattern formation and the distribution of $\phi_i^{(1)}$. (a) The pattern formation when $\varepsilon = 1, \beta = 0.0449$ and $Re(c_1(\beta)) = -0.0070 < 0$.(b) The pattern formation when $\varepsilon = 1, \beta = 0.035 < \beta_c$ and $Re(c_1(\beta)) = -0.0038 < 0$. (c) The distribution of $\phi_i^{(1)}$ for Laplacian matrix $\varepsilon = 1$.

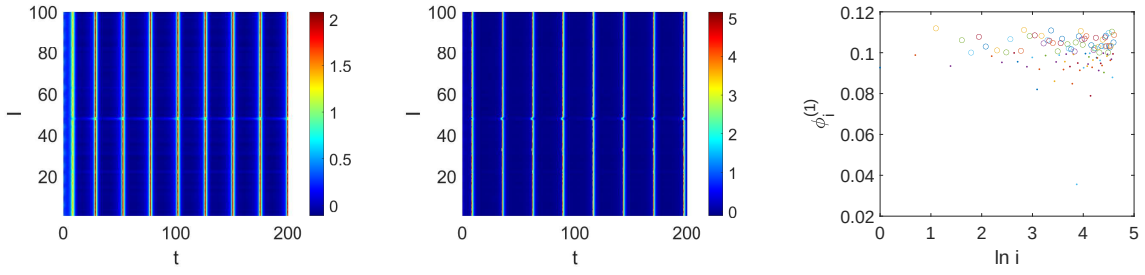

Figure 8. The pattern formation and the distribution of $\phi_i^{(1)}$. (a) The pattern formation when $\varepsilon = 0.8, \beta = 0.035$ and $Re(c_1(\beta)) = 0.0017 > 0$. (b) The pattern formation when $\varepsilon = 0.8, \beta = 0.01$ and $Re(c_1(\beta)) = 0.0137 > 0$. (c) The distribution of $\phi_i^{(1)}$ for Quasi-Laplacian matrix $\varepsilon = 0.8$.

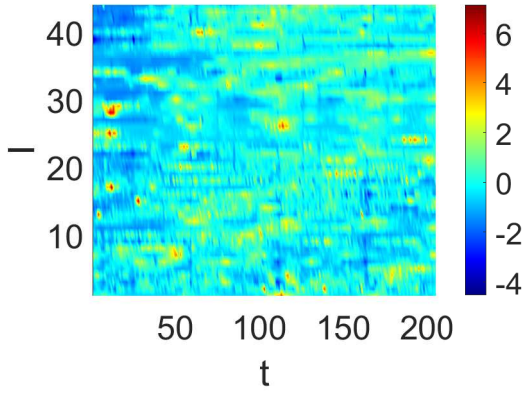

Figure 9. The new confirmed cases about influenza in Africa, Eastern Mediterranean and Western Pacific regions from 11.14.2021 to 10.12.2025. Data source: FluNet (https://www.who.int/tools/flunet).

5. Conclusion

In this paper, we proposed a network-organized SIR epidemic model that integrates indirect transmission mechanisms with quasi-Laplacian diffusion to capture the interplay between biological processes and network-connected mobility. By conducting linear stability analysis, eigenmode decomposition, and normal-form reduction, we derived explicit parameter thresholds governing Hopf bifurcation, Turing instability, and their interaction within heterogeneous networks. The analytical results reveal that indirect transmission reshapes epidemic thresholds and can trigger oscillatory outbreaks even when direct transmission remains insufficient to destabilize the endemic equilibrium. Meanwhile, asymmetric diffusion between susceptible and infected populations enlarges Turing-unstable regions and activates additional network eigenmodes, giving rise to spatially heterogeneous infection patterns.

Numerical simulations further substantiate these theoretical findings. In the absence of network effects, the system exhibits clear transitions among disease-free, endemic, and periodic states as key biological parameters cross bifurcation thresholds. When embedded in random or quasi-Laplacian networks, the system displays a rich repertoire of spatiotemporal dynamics, including spatially synchronized oscillations, nonuniform periodic outbreaks, coexistence of endemic and oscillatory nodes, and complex Turing-Hopf interactions. The results also indicate that network connectivity, node degree heterogeneity, and the strength of diffusion asymmetry decisively shape the number and type of unstable modes, thereby determining the emergence and spatial form of epidemic clusters.

To validate the theoretical framework, we calibrated the model using real influenza surveillance data collected from 44 countries in Africa, the Eastern Mediterranean, and the Western Pacific between 2021 and 2025. The empirical data exhibit pronounced periodicity and spatial clustering-features accurately reproduced by the model's Hopf and Turing bifurcation mechanisms. This agreement demonstrates that instability-driven processes, amplified by asymmetric mobility and indirect transmission pathways, can explain the recurrent cycles and regional heterogeneity observed in real-world influenza outbreaks.

Overall, this study establishes a comprehensive theoretical and data-supported foundation for understanding epidemic pattern formation in structured populations. It highlights that reducing indirect transmission routes, managing asymmetric mobility, or reshaping network

connectivity can effectively suppress instability-driven oscillations and spatial clustering. These insights provide valuable guidance for designing control strategies in modern, mobility-connected epidemiological environments.

Acknowledgements

The authors would like to express sincere gratitude to the anonymous referees for their valuable comments and constructive suggestions, which have greatly improved the quality of this paper.

Appendix A

Appendix A1

The detailed presentation of the expressions $p_{21}, p_{22}, p_{23}, p_{24}, p_{25}, p_{26}, q_{21}, q_{22}, q_{23}, q_{24}, q_{25}$

$$
\begin{aligned}
p_{21} &= d_I(d_I + d_S),\\
p_{22} &= (2d_I + d_S)(uv\gamma - \delta) - d_I(v^2\gamma + 2\beta u) - (d_I - d_S)ib(\beta_c),\\
p_{23} &= (4u^2v^2 - 2uv^3)\gamma^2 - 2(2u^2\beta + (ib(\beta_c) + 2\delta)u + \frac{(ib(\beta_c) - \delta)v}{2})v\gamma - 2\beta(ib(\beta_c) - \delta)u\\
&\quad + ib(\beta_c)\delta + \delta^2 + 2(b(\beta_c))^2,\\
p_{24} &= (d_I + d_S)^2,\\
p_{25} &= 4(d_I + d_S)((u - \frac{v}{2})v\gamma - \beta u - \frac{\delta}{2}),\\
p_{26} &= 4(u - \frac{v}{2})^2v^2\gamma^2 - 8(\beta u + \frac{\delta}{2})(u - \frac{v}{2})v\gamma + 4\beta^2u^2 + 4\beta\delta u + \delta^2 + 4(b(\beta_c))^2,\\
q_{21} &= 2(d_I + d_S)uv\gamma,\\
q_{22} &= -4((-u + \frac{v}{2})v\gamma + \beta u + ib(\beta_c) + \frac{\delta}{2})uv\gamma,\\
q_{23} &= (d_I + d_S)^2,\\
q_{24} &= 4(d_I + d_S)((u - \frac{v}{2})v\gamma - \beta u - \frac{\delta}{2}),\\
q_{25} &= 4(u - \frac{v}{2})^2v^2\gamma^2 - 8(\beta u + \frac{\delta}{2})(u - \frac{v}{2})v\gamma + 4\beta^2u^2 + 4\beta\delta u + \delta^2 + 4(b(\beta_c))^2.
\end{aligned}
$$

Appendix A2

The detailed presentation of the expressions $a_{ij}(i = 1, 2, 3, 4, 5, 6, j = 1, 2, 3)$

$$
\begin{aligned}
a_{11} &= -\frac{{d_S}^2}{2\,\gamma\,uv^2},\\
a_{12} &= \frac{-d_S}{u} + \frac{2\,d_S\,\beta}{\gamma\,v^2} + \frac{d_S\,ib(\beta_c)}{\gamma\,uv^2},\\
a_{13} &= \frac{3\gamma\,v^2}{2u} + \frac{ib(\beta_c)}{u} - \frac{2\,u\beta^2}{\gamma\,v^2} - \frac{2\,\beta\,ib(\beta_c)}{\gamma\,v^2} + \frac{b(\beta_c)^2}{2\,\gamma\,uv^2},\\
a_{21} &= \frac{{d_S}^2}{2\,\gamma\,uv^2},
\end{aligned}
$$

$$
\begin{aligned}
a_{22} &= \frac{d_S}{u} - \frac{d_S\, ib(\beta_c)}{\gamma\, uv^2} - \frac{2\, d_S\, \beta}{\gamma\, v^2},\\
a_{23} &= -\frac{3\gamma\, v^2}{2\, u} - \frac{ib(\beta_c)}{u} + \frac{2\, u\beta^2}{\gamma\, v^2} + \frac{2\, \beta\, ib(\beta_c)}{\gamma\, v^2} - \frac{b(\beta_c)^2}{2\, \gamma\, uv^2},\\
a_{31} &= -\frac{{d_S}^2}{2\, \gamma\, uv^2},\\
a_{32} &= \frac{-d_S}{u} + \frac{2\, d_S\, \beta}{\gamma\, v^2},\\
a_{33} &= \frac{3\gamma\, v^2}{2\, u} - \frac{2\, u\beta^2}{\gamma\, v^2} - \frac{b(\beta_c)^2}{2\, \gamma\, uv^2},\\
a_{41} &= \frac{{d_S}^2}{2\, \gamma\, uv^2},\\
a_{42} &= \frac{d_S}{u} - \frac{2d_S\, \beta}{\gamma\, v^2},\\
a_{43} &= -\frac{3\, \gamma\, v^2}{2\, u} + \frac{2\, u\beta^2}{\gamma\, v^2} + \frac{b(\beta_c)^2}{2\, \gamma\, uv^2},\\
a_{51} &= -\frac{3\, {d_S}^2}{2\, \gamma\, u^2v^2},\\
a_{52} &= \frac{3\, d_S}{u^2} + \frac{6\, d_S\, \beta}{\gamma\, uv^2} + \frac{d_S\, ib(\beta_c)}{\gamma\, u^2v^2},\\
a_{53} &= -\frac{3\, \gamma\, v^2}{2\, u^2} - \frac{6\, \beta}{u} - \frac{6\, \beta^2}{\gamma\, v^2} - \frac{b(\beta_c)^2}{2\, \gamma\, u^2v^2} - \frac{ib(\beta_c)}{u^2} - \frac{2\, \beta\, ib(\beta_c)}{\gamma\, uv^2},\\
a_{61} &= \frac{3\, {d_S}^2}{2\, \gamma\, u^2v^2},\\
a_{62} &= -\frac{3\, d_S}{u^2} - \frac{6\, d_S\, \beta}{\gamma\, uv^2} - \frac{d_S\, ib(\beta_c)}{\gamma\, u^2v^2},\\
a_{63} &= \frac{3\, \gamma\, v^2}{2\, u^2} + \frac{6\, \beta}{u} + \frac{6\, \beta^2}{\gamma\, v^2} + \frac{b(\beta_c)^2}{2\, \gamma\, u^2v^2} + \frac{ib(\beta_c)}{u^2} + \frac{2\, \beta\, ib(\beta_c)}{\gamma\, uv^2}.
\end{aligned}
$$

Appendix A3

The detailed presentation of the expressions $s_3, s_4, b_{ij}(i = 1, 2, 3, 4, 5, j = 1, 2, 3), b_{54}$

$$
\begin{aligned}
s_3 &= \sum_{i=1}^{n} (\phi_i^{(1)})^3, s_4 = \sum_{i=1}^{n} (\phi_i^{(1)})^4,\\
b_{11} &= 2\, \gamma\, uv^2 \left(2\, \gamma\, uv - \gamma\, v^2 + \Lambda\, d_S + \Lambda\, d_I - 2\, \beta\, u - \delta - 2ib(\beta_c)\right),\\
b_{12} &= -3\, \gamma^2 v^4 + 2\, \Lambda\, d_S\, \gamma\, v^2 - 2\, \gamma\, v^2 ib(\beta_c) + \Lambda^2 {d_S}^2 - 2\, \Lambda\, d_S ib(\beta_c)\\
&\quad - 4\, \Lambda\, \beta\, d_S\, u - b(\beta_c)^2 + 4\, \beta\, ib(\beta_c)\, u + 4\, \beta^2 u^2,\\
b_{13} &= -d_I \Lambda + ib(\beta_c) + \delta,\\
b_{21} &= 2\, \gamma\, uv^2 \left(2\, \gamma\, uv - \gamma\, v^2 + \Lambda\, d_S + \Lambda\, d_I - 2\, \beta\, u - \delta + 2ib(\beta_c)\right),\\
b_{22} &= -3\, \gamma^2 v^4 + 2\, \Lambda\, d_S\, \gamma\, v^2 - 2\, \gamma\, v^2 ib(\beta_c) + \Lambda^2 {d_S}^2 - 2\, \Lambda\, d_S ib(\beta_c)\\
&\quad - 4\, \Lambda\, \beta\, d_S\, u - b(\beta_c)^2 + 4\, \beta\, ib(\beta_c)\, u + 4\, \beta^2 u^2,
\end{aligned}
$$

$$
\begin{aligned}
b_{23} &= -d_I\Lambda - ib(\beta_c) + \delta,\\
b_{31} &= 2\,\gamma\,uv^2\left(2\,\gamma\,uv - \gamma\,v^2 + \Lambda\,d_S + \Lambda\,d_I - 2\,\beta\,u - \delta - 2ib(\beta_c)\right),\\
b_{32} &= -3\,\gamma^2v^4 + 2\,\Lambda\,d_S\,\gamma\,v^2 + \Lambda^2{d_S}^2 - 4\,\Lambda\,\beta\,d_S\,u + 4\,\beta^2u^2 + b(\beta_c)^2,\\
b_{33} &= -d_I\Lambda + ib(\beta_c) + \delta,\\
b_{41} &= 2\,\gamma\,uv^2\left(2\,\gamma\,uv - \gamma\,v^2 + \Lambda\,d_S + \Lambda\,d_I - 2\,\beta\,u - \delta + 2ib(\beta_c)\right),\\
b_{42} &= -3\,\gamma^2v^4 + 2\,\Lambda\,d_S\,\gamma\,v^2 + \Lambda^2{d_S}^2 - 4\,\Lambda\,\beta\,d_S\,u + 4\,\beta^2u^2 + b(\beta_c)^2,\\
b_{43} &= -d_I\Lambda - ib(\beta_c) + \delta,\\
b_{51} &= 2\,\gamma\,uv^2\left(2\,\gamma\,uv - \gamma\,v^2 + \Lambda\,d_S + \Lambda\,d_I - 2\,\beta\,u - \delta - 2ib(\beta_c)\right),\\
b_{52} &= -\gamma\,v^2 + d_S\,\Lambda - ib(\beta_c) - 2\,\beta\,u,\\
b_{53} &= -3\,\gamma\,v^2 + 3\,d_S\,\Lambda + ib(\beta_c) - 6\,\beta\,u,\\
b_{54} &= -d_I\Lambda + ib(\beta_c) + \delta.
\end{aligned}
$$

Appendix A4

The specific derivation process of the formula (3.9)

$$
\begin{aligned}
\frac{dz}{dt} &= ib(\beta_c)z + \langle p^*, N_c\rangle\\
&= ib(\beta_c)z + \langle p^*, \frac{1}{2}K(C,C) + \frac{1}{6}M(C,C,C)\rangle\\
&= ib(\beta_c)z + \frac{1}{2}\langle p^*, K(zp+\overline{zp}+\omega, zp+\overline{zp}+\omega)\rangle\\
&\quad + \frac{1}{6}\langle p^*, M(zp+\overline{zp}+\omega, zp+\overline{zp}+\omega, zp+\overline{zp}+\omega)\rangle\\
&= ib(\beta_c)z + \frac{1}{2}z^2\langle p^*, K(p,p)\rangle + z\overline{z}\langle p^*, K(p,\overline{p})\rangle + \frac{1}{2}\overline{z}^2\langle p^*, K(\overline{p},\overline{p})\rangle\\
&\quad + z\langle p^*, K(p,\omega)\rangle + \overline{z}\langle p^*, K(\overline{p},\omega)\rangle + \frac{1}{6}z^3\langle p^*, M(p,p,p)\rangle\\
&\quad + \frac{1}{2}z^2\overline{z}\langle p^*, M(p,p,\overline{p})\rangle + \frac{1}{2}z\overline{z}^2\langle p^*, M(p,\overline{p},\overline{p})\rangle\\
&\quad + \frac{1}{6}\overline{z}^3\langle p^*, M(\overline{p},\overline{p},\overline{p})\rangle + O(|z|^4)\\
&= ib(\beta_c)z + \frac{1}{2}z^2\langle p^*, K(p,p)\rangle + z\overline{z}\langle p^*, K(p,\overline{p})\rangle + \frac{1}{2}\overline{z}^2\langle p^*, K(\overline{p},\overline{p})\rangle\\
&\quad + \frac{1}{2}z^3\langle p^*, K(p,\omega_{20})\rangle + z^2\overline{z}\langle p^*, K(p,\omega_{11})\rangle + \frac{1}{2}z\overline{z}^2\langle p^*, K(p,\omega_{02})\rangle\\
&\quad + \frac{1}{2}z^2\overline{z}\langle p^*, K(\overline{p},\omega_{20})\rangle + z\overline{z}^2\langle p^*, K(\overline{p},\omega_{11})\rangle + \frac{1}{2}\overline{z}^3\langle p^*, K(\overline{p},\omega_{02})\rangle\\
&\quad + \frac{1}{6}z^3\langle p^*, M(p,p,p)\rangle + \frac{1}{2}z^2\overline{z}\langle p^*, M(p,p,\overline{p})\rangle\\
&\quad + \frac{1}{2}z\overline{z}^2\langle p^*, M(p,\overline{p},\overline{p})\rangle + \frac{1}{6}\overline{z}^3\langle p^*, M(\overline{p},\overline{p},\overline{p})\rangle + O(|z|^4)\\
&= ib(\beta_c)z + \frac{1}{2}z^2\langle p^*, K(p,p)\rangle + z\overline{z}\langle p^*, K(p,\overline{p})\rangle + \frac{1}{2}\overline{z}^2\langle p^*, K(\overline{p},\overline{p})\rangle
\end{aligned}
$$

$$
\begin{aligned}
&+\frac{1}{6}z^3\left(3\langle p^*,K(p,\omega_{20})\rangle+\langle p^*,M(p,p,p)\rangle\right)\\
&+\frac{1}{2}z^2\overline{z}\left(2\langle p^*,K(p,\omega_{11})\rangle+\langle p^*,K(\overline{p},\omega_{20})\rangle+\langle p^*,M(p,p,\overline{p})\rangle\right)\\
&+\frac{1}{2}z\overline{z}^2\left(2\langle p^*,K(\overline{p},\omega_{11})\rangle+\langle p^*,K(p,\omega_{02})\rangle+\langle p^*,M(p,\overline{p},\overline{p})\rangle\right)\\
&+\frac{1}{6}\overline{z}^3\left(3\langle p^*,K(\overline{p},\omega_{02})\rangle+\langle p^*,M(\overline{p},\overline{p},\overline{p})\rangle\right)+O(|z|^4)\\
=\;&ib(\beta_c)z+\frac{1}{2}g_{20}z^2+g_{11}z\overline{z}+\frac{1}{2}g_{02}\overline{z}^2+\frac{1}{6}g_{30}z^3\\
&+\frac{1}{2}g_{21}z^2\overline{z}+\frac{1}{2}g_{12}z\overline{z}^2+\frac{1}{6}g_{03}\overline{z}^3+O(|z|^4).
\end{aligned}
$$

References

[1] R. M. Anderson and R. M. May, *Infectious Diseases of Humans: Dynamics and Control*, Oxford Univ. Press, 1991.

[2] M. Asllani, J. D. Challenger, F. S. Pavone, L. Sacconi and D. Fanelli, *The theory of pattern formation on directed networks*, Nat. Commun., 2014, 5, 4517.

[3] M. Chen and X. Li, *Stability analysis and Turing pattern of an enzyme-catalyzed reaction model*, Nonlinear Anal. Real World Appl., 2025, 94(1), 195–214.

[4] W. Gou, Z. Jin and H. Wang, *Hopf bifurcation for general network-organized reaction-diffusion systems and its application in a multi-patch predator-prey system*, J. Differ. Eqs., 2023, 346, 64–107.

[5] R. Khan, I. L. Popa, E. A. A. Ismail and others, *Deterministic and fractional-order modeling of measles dynamics with harmonic mean incidence rate and quarantine impact*, Sci. Rep., 2025, 15, 30597.

[6] Y. A. Kuznetsov, *Elements of Applied Bifurcation Theory*, Springer, New York, 1995.

[7] N. M. Manshouri, *Identifying COVID-19 by using spectral analysis of cough recordings: A distinctive classification study*, Cogn. Neurodyn., 2022, 16(1), 239–253.

[8] H. Nakao and A. S. Mikhailov, *Turing patterns in network-organized activator-inhibitor systems*, Nat. Phys., 2010, 6, 544–550.

[9] L. Pei, *Prediction of numbers of the accumulative confirmed patients (NACP) and the plateau phase of 2019-nCoV in China*, Cogn. Neurodyn., 2020, 14(3), 411–424.

[10] L. Pei and M. Zhang, *Long-term predictions of current confirmed and dead cases of COVID-19 in China by the non-autonomous delayed epidemic models*, Cogn. Neurodyn., 2022, 16(1), 229–238.

[11] A. M. Turing, *The chemical basis of morphogenesis*, Philos. Trans. R. Soc. B, 1952, 237, 37–72.

[12] Z. Wang, C. Xia, Z. Chen and G. Chen, *Epidemic propagation with positive and negative preventive information in multiplex networks*, IEEE Trans. Cybern., 2021, 51(3), 1454–1462.

[13] S. Zhai, J. Zhang, J. Ma and Z. Xiang, *Cluster synchronization of individuals during an epidemic: A contraction-based analysis*, IEEE Trans. Syst. Man Cybern. Syst., 2025, 55(10), 6868–6878.

[14] H. Zhang, J. Gao, C. Gu, C. Shen and H. Yang, *Transition and coexistence of Turing pattern, Turing-like pattern and spiral waves in a discrete-time predator-prey model*, Chaos Solitons Fractals, 2024, 189, 115591.

[15] X. Zhang and Z. Liu, *Hopf bifurcation for a susceptible-infective model with infection-age structure*, J. Nonlinear Sci., 2020, 30, 317–367.

[16] Y. Zhang, S. Ruan and T. Zhang, *Turing-Hopf bifurcation in diffusive epidemic models*, J. Differ. Eqs., 2017, 263(12), 8541–8576.

[17] Y. Zhang and X. Wu, *Dynamic behavior and sliding mode control on a stochastic epidemic model with alertness and distributed delay*, Commun. Nonlinear Sci. Numer. Simul., 2023, 124, 107299.

[18] Q. Zheng and others, *Pattern dynamics in the epidemic model with diffusion network*, EPL, 2022, 137, 42002.

[19] Q. Zheng and others, *Network topology and double delays in Turing instability and pattern formation*, J. Phys. A: Math. Theor., 2024, 57, 395203.

[20] Q. Zheng and others, *Pattern selection mechanism from the equilibrium point and limit cycle*, Chaos, 2024, 34, 023124.

[21] Q. Zheng and others, *Spatiotemporal dynamics of periodic waves in SIR model with driving factors*, New J. Phys., 2023, 25, 063028.

[22] Q. Zheng, J. Shen, V. Pandey, L. Guan and Y. Guo, *Turing instability in a network-organized epidemic model with delay*, Chaos Solitons Fractals, 2023, 168, 113205.

[23] L. Zhu, Y. Ding and S. Shen, *Green behavior propagation analysis based on statistical theory and intelligent algorithm in data-driven environment*, Math. Biosci., 2025, 379, 109340.

[24] L. Zhu, G. Guan and Y. Li, *Nonlinear dynamical analysis and control strategies of a network-based SIS epidemic model with time delay*, Appl. Math. Model., 2019, 70, 512–531.

[25] L. Zhu and Y. Li, *Dynamic propagation and control of a West Nile virus model based on higher-order temporal network structure*, Phys. Rev. E, 2025, 112, 044409.

[26] L. Zhu, Y. Li, L. He and S. Shen, *Pattern formation of network epidemic model and its application in oral medicine*, Comput. Methods Programs Biomed., 2025, 264, 108688.

[27] L. Zhu and T. Zheng, *Pattern dynamics analysis and application of West Nile virus spatiotemporal models based on higher-order network topology*, Bull. Math. Biol., 2025, 87, 121.

Received November 2025; Accepted February 2026; Available online February 2026.